



**University of Dundee**

## **REAL-TIME RASTERIZATION SIMULATION OF TIR IMAGES**

Vural, Deren; Martin, Iain; Dunstan, Martin; Sanchez-Gestido, Manuel

*Publication date:*  
2023

[Link to publication in Discovery Research Portal](#)

*Citation for published version (APA):*

Vural, D., Martin, I., Dunstan, M., & Sanchez-Gestido, M. (2023). *REAL-TIME RASTERIZATION SIMULATION OF TIR IMAGES*. Paper presented at 12th International Conference on Guidance, Navigation & Control Systems (GNC), Sopot, Poland.

### **General rights**

Copyright and moral rights for the publications made accessible in Discovery Research Portal are retained by the authors and/or other copyright owners and it is a condition of accessing publications that users recognise and abide by the legal requirements associated with these rights.

### **Take down policy**

If you believe that this document breaches copyright please contact us providing details, and we will remove access to the work immediately and investigate your claim.

## REAL-TIME RASTERIZATION SIMULATION OF TIR IMAGES

**Deren Vural<sup>(1)</sup>, Iain Martin<sup>(1)</sup>, Martin Dunstan<sup>(1)</sup>, Manuel Sanchez-Gestido<sup>(2)</sup>**

<sup>(1)</sup>*University of Dundee, Dundee, DD1 4HN, United Kingdom, d.vural@dundee.ac.uk*

<sup>(2)</sup>*University of Dundee, Dundee, DD1 4HN, United Kingdom, i.martin@dundee.ac.uk*

<sup>(3)</sup>*University of Dundee, Dundee, DD1 4HN, United Kingdom, m.n.dunstan@dundee.ac.uk*

<sup>(2)</sup>*ESTEC, ESA, Noordwijk, The Netherlands, Manuel.Sanchez.Gestido@esa.int*

### ABSTRACT

Thermal/Infrared (TIR) sensors are being considered for Guidance, Navigation and Control (GNC) systems, in addition to the existing roster of visible light spectrum (VIS) sensors. The real-time generation of synthetic data used to supplement and extend existing datasets used in closed-loop testing should also be extended to the TIR spectral range. For spacecraft this has previously been limited to ‘stateless’ methods in rasterisation based systems, i.e. with no consideration of TIR effects that occur over time, such as thermal conduction and thermal capacitance; or to computationally expensive methods in more traditional engineering software, such as Monte-Carlo based ray tracing and Finite Element Analysis (FEA).

This paper reports on the progress of a technique being developed for synthetic TIR image generation in rasterisation based systems: a ‘capacitance model’ that involves the creation of a Thermal Mathematical Model (TMM), to keep track of the temperature of each node, and the assignment of thermal properties to each node. This allows the examination of the time-based thermal-infrared (TIR) effect of thermal inertia (also known as thermal lag), a result of thermal mass that affects the temperature change of an object as the input and/or output energy changes i.e. during transient stages of heat transfer. An OpenGL prototype was developed, aiming to recreate a set of thermal inertia functions to show how simulation of this effect can improve the accuracy of real-time generated images, in particular during the simulation of important transitional phases of spacecraft orbits, e.g. the entry or exit of eclipse. Mathematical functions can be used to effectively simulate time-based thermal inertia as an extension of previously used standard thermal equations, and in future these functions could be combined to simulate complex thermal profiles, e.g. those of a spacecraft in planetary orbit.

## 1 INTRODUCTION

As Thermal/Infrared (TIR) sensors have become lighter and more advanced, and thus increasingly useful, they are being considered for Guidance, Navigation and Control (GNC) systems, in addition to the existing roster of visible light spectrum (VIS) cameras and LiDAR sensors. A crucial step in the development of GNC systems is the testing of sensor systems including analysis methods that utilise sensor data, which requires large data sets of images. Although there are plenty of data sets in VIS, synthetic data has been widely used to supplement and extend to provide additional datasets with customisable parameters including roughness, feature distributions and lighting scenarios. In order to expedite this process, VIS image generation software such as the Planet and Asteroid Natural Generation Utility (PANGU) [1] and Airbus's SurRender [2] are used to generate synthetic images representative of the kind of data that would be gathered. For spacecraft this was previously limited to the VIS spectral range, but as a result of the development in TIR sensors, methods of generating representative synthetic TIR images of spacecraft are now required to aid in development and testing. An important requirement of synthetic image generation for use in GNC development is the aspect of 'real time' image generation for the purpose of closed-loop testing. This is usually done at a speed of around around 10Hz, to match the rate of sensor data generated in spacecraft and landers. With the expansion of spacecraft GNC sensor suites into the TIR range, there is now a requirement for realistic and accurate generation of synthetic TIR images at real-time speeds.

This paper reports on the progress of the first of two techniques being developed for synthetic TIR image generation: a 'capacitance model' that involves the creation of a Thermal Mathematical Model (TMM) to keep track of the temperature of each node, and the assignment of thermal properties to each node. Varying by material density, thermal reflectance, and thermal conductivity, the thermal inertia of a material defines how long it takes for a material to absorb and release thermal energy: for example aluminium takes longer to heat than copper, but will also hold on to that thermal energy for a longer time-period, slowly releasing it in the form of thermal radiation and conduction. The effects generated by this system in TIR images are most crucial during fast thermal transitions, e.g. the entry and exit of eclipse, or the activation/deactivation of a thermal control system e.g. a heater or radiator system. This method could be used with multiple material types to improve the accuracy of simulations involving complex models, e.g. large spacecraft like the International Space Station (ISS) in image generation software.

Image generation software attempt to create visually accurate and representative images of surfaces. This is in contrast to traditional thermal analysis tools, like ESATAN-TMS [3] which aim to accurately calculate interior temperatures given boundary conditions and equipment limits, and more modern engineering CAD software, e.g. SolidWorks [4], which perform similar types of calculations but usually within atmosphere using modern Finite Element Analysis (FEA) techniques. These more traditional engineering analysis tools are not designed for the real-time generation of images, and are functionally difficult to use for GNC development being more focussed on the design of components and material analysis.

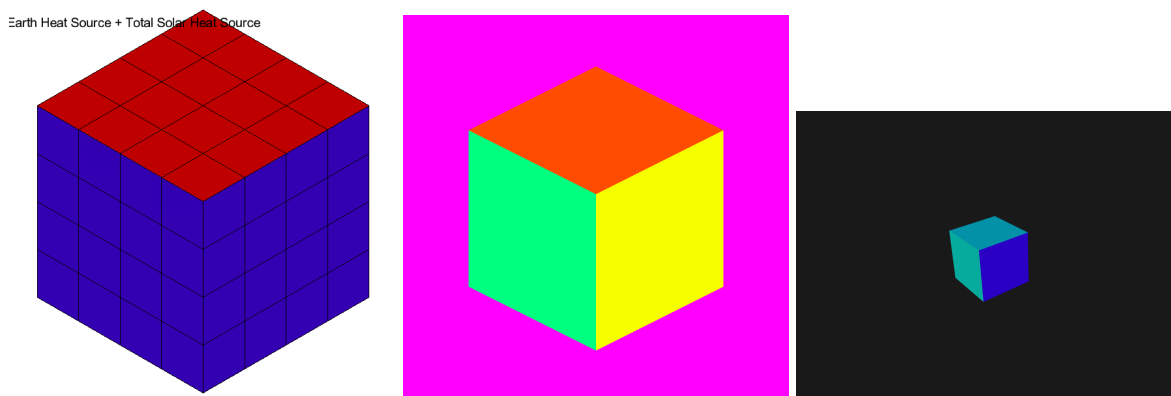


Figure 1: Simplified cubesat model in 1: ESATAN, 2: PANGU, 3: Prototype

## 2 BACKGROUND

Traditional thermal analysis is performed using Finite Difference (also called Lumped Parameter) and FEA techniques that utilize standard heat transfer equations tailored for spacecraft in custom-made software tools like ESATAN-TMS [3]. CAD software like SolidWorks [4] have expanded to simulate thermal systems using modern FEA techniques, though few take into account the orbital nature of spacecraft and the change in energy across these orbits. For this reason, ESATAN-TMS's [3] orbital module ensures it stands as one of the few tools available for directly simulating spacecraft thermal behaviour. To design a system that models thermal inertia, we can use the temperature profiles extracted from ESATAN-TMS [3] simulations as a basis for our own, making note of discrepancies.

To generate representative images in the TIR spectral range, we can adapt techniques from traditional thermal analysis software to more flexible rendering tools like PANGU [1], which generates representative images using efficient and fast traditional rendering techniques over computationally expensive techniques like FEA. A real-time but thermally 'stateless', i.e. with no record of previous state or consideration of thermal effects that occur over time, model was developed for PANGU v6.0 using traditional thermal analysis equations during the generation of each frame in the simulation [5]. However, there remain some discrepancies in the thermal profile (and thus images) generated using this technique [5], possibly because it functions without any consideration of changes that occur over more than a single frame.

### 2.1 ESATAN-TMS

Using ESATAN-TMS [3], we can simulate a range of thermal materials to better understand their thermal behaviour. Across an ESATAN-TMS simulated orbit, sections of the chosen model will heat and cool according to the constituent thermal properties of the material they are made from as well as the input angle of the Sun. This allows an increased understanding of the radiated TIR response of the surfaces, and the temperatures generated (as well as estimated generated radiance values) can be plotted which can then be used to design the response i.e. the 'thermal profile' of a material given some solar input.

To maintain consistency and reduce complexity, an orbit of 224km and orbital period of around 6017s was used, with the Sun set to be on the orbital plane (i.e. a beta angle of zero degrees). Within

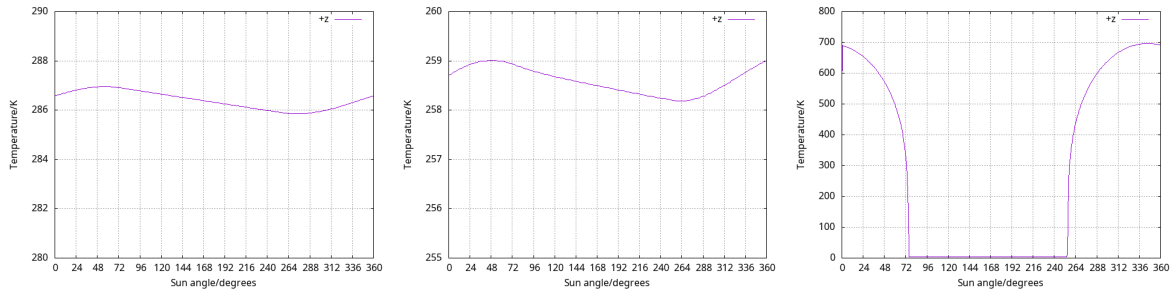


Figure 2: 1: ESATAN Solar graph for +Z face using Aluminium material (radiation enabled only, with a Y scale of 0K-290K), 2: ESATAN Solar graph for +Z face using Aluminium material (radiation and conduction enabled, with a Y scale of 0K-260K), 3: ESATAN Solar graph for +Z face in MLI material (radiation enabled only, with a Y scale of 0K-800K)

ESATAN-TMS this was sampled using a time-step of around 17s dividing the orbit into 360 time-steps. An equivalent scenario was simulated in PANGU and the prototype system by using 360 different solar input angles, as the light sources within these systems require only input angle to calculate solar input unlike ESATAN-TMS. The number of time-steps within ESATAN-TMS was limited due in part to memory requirements of the thermal solver during these simulations. The ESATAN-TMS model was designed as a simplified hollow cube shape (see Figure 1), using a thickness of 0.1m for each panel which measure 1m by 1m. For the material properties used, see Tables 1 and 2.

In Figure 2, the temperature variation across a single orbit can be seen for the space-facing (aka +Z plane or zenith) face of an earth-orbiting spacecraft (see Figure 1 for an image of the spacecraft model), using the Aluminium and MLI materials. The orbit, and thus input radiation, are the same for both material models, with the eclipse occurring between time-steps 75 and 250, roughly 175 time-steps of the orbit.

1. In the MLI plot of Figure 2, the period of temperature rise of the panel can be seen between around time-steps 250 and 340, roughly 90–100 time-steps. The period of temperature drop of the panel can be seen between timesteps 340 and 72, roughly 90 time-steps.
2. In the Aluminium plot of Figure 2, the period of temperature rise of the panel can be seen between around timesteps 270 and 50, roughly 140–150 time-steps. The period of temperature drop of the panel can be seen between around timesteps 50 and 270, roughly 220 time-steps.

These differences demonstrate much longer periods of temperature rise and (even longer) periods of temperature drop for Aluminium than MLI, which is to be expected due to the higher density and heat capacity (and thus thermal mass) of Aluminium. This notably occurs across a very small amplitude of 1K, again likely a product of the higher density and heat capacity (and thus thermal mass) of Aluminium. The very low density and functionally zero heat capacity (and thus thermal mass) of MLI clearly show themselves here, with temperature variations across an amplitude of 700K. These effects are visible in the much longer period of temperature drop, as the energy stored within the Aluminium slowly dissipates in the form of radiation to space while the MLI cools to background temperature for the entire eclipse. With other forms of heat transfer (such as conduction) enabled, the period of temperature drop for the Aluminium model occurs only a little faster (see steeper curves of image two of Figure 2), while the MLI responds almost instantaneously to temperature changes (see image three of Figure 2).

Table 1: ESATAN-TMS Optical Material Properties

Material	Emissivity ( $\epsilon$ )	Absorptivity ( $\alpha$ )
Aluminium 6061	0.21	0.18
Goldized MLI	0.02	0.19

Table 2: ESATAN-TMS Material Properties

Material	Conductivity (W/m·K)	Density (kg/m <sup>3</sup> )	Specific Heat Capacity (J/kg·K)
Aluminium 6061	200	2700	900
Goldized MLI	0.01	0	0

## 2.2 PANGU

PANGU [1] focuses on the emissivity and absorptivity of the model, using thermal equations from [6], and due to being a real-time, stateless rasterisation system, focuses entirely on the surface (radiative) response rather than simulating the entire solid object. Using PANGU, we can re-create this simulation with the same CAD model and some of the thermal properties of the materials used to highlight the gap in ability of the stateless thermal method that we aim to enhance. In most general conditions this succeeds as shown in Figure 3. The standard thermal equations of [6] allow a good accuracy in a singular, stateless moment, like peak solar input radiation for the +Z face (i.e. around time-step 340).

However, where other thermal effects become more important than incoming radiation, i.e. entry/exit and duration of eclipse, the temperatures generated using PANGU and ESATAN begin to diverge slightly. As shown in Figure 4, the shapes of the temperatures curves can be seen to differ slightly, and this is especially clear as the model exits eclipse (and thus thermal equilibrium of around 180K) near time-step 264. This lower ‘resting’ (thermal equilibrium) temperature during eclipse in the PANGU model is likely due to lack of time-based thermal effects like thermal inertia and conduction.

## 2.3 Requirements

The thermal profile differences outlined in Sections 2.1 and 2.2 allow the definition of a clear set of temperature functions that should be created in the prototype system, in order to improve thermal simulation accuracy:

1. The ESATAN-TMS Aluminium material model (see Figure 2) features a slow temperature rise and drop period across 1K in the upper 200K range over a gradual curve, likely due to the relatively higher thermal mass (and thus thermal capacitance) resulting in a stronger thermal inertia effect
2. Sections of the thermal profile of the ESATAN-TMS Aluminium material model also seem almost linear (see Figure 2)
3. The ESATAN-TMS MLI material model (see Figure 2) features steep temperature rise and drop periods between 0K and 700K, likely due to the relatively low thermal mass removing most of the thermal inertia effect

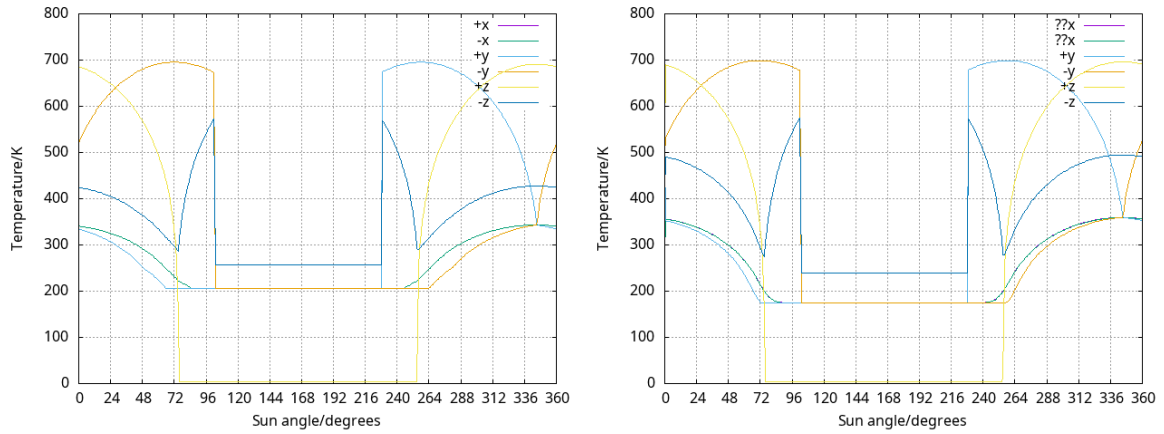


Figure 3: 1: PANGU model all faces, using MLI material (Background, Solar, Albedo and Planetary input radiation enabled) 2: ESATAN model all face, using MLI material (Background, Solar, Albedo and Planetary input radiation enabled)

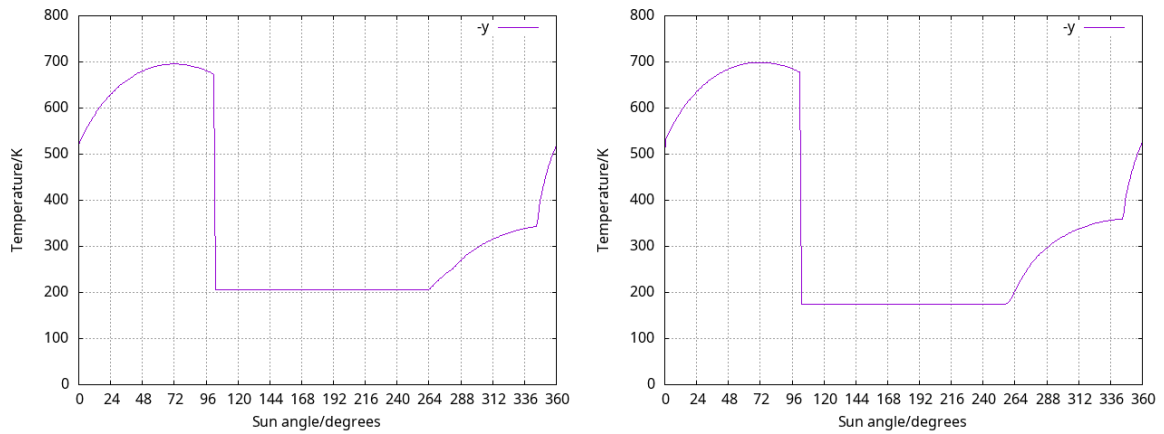


Figure 4: 1: PANGU model +Y face, using MLI material (Background, Solar, Albedo and Planetary input radiation enabled), 2: ESATAN +Y face, using MLI material (Background, Solar, Albedo and Planetary input radiation enabled)

4. The PANGU MLI material model (see Figure 4) features sharp changes during transition periods (around time-step 264) when compared to the equivalent ESATAN simulation, though this could be attributed to interpolation effects due to the sampling of time-steps in both PANGU and ESATAN

These curves could be approximated using combinations of linear and quadratic functions, with consideration of environmental conditions and initial temperatures defining these functions. Building a system to simulate temperature profiles in this manner could allow the extension of stateless thermal simulations (e.g. PANGU) to more accurately simulate both complex temperature transitions and temperature ‘equilibriums’ that stay within stable temperature ranges.

### 3 PROTOTYPE IMPLEMENTATION

#### 3.1 Prototype Design

In order to properly test various mathematical functions in the generation of a thermal inertia effect in generated temperature curves, a prototype was developed in OpenGL utilizing standard thermal equations [6] to simulate temperature, and radiance conversion equations to properly simulate the expected generated TIR sensor image. The user has the choice of images which can be calibrated to generate radiance images, or false-colour temperature values which useful for understanding thermal effects and gradients. The prototype calculates temperature at the vertex level, which is interpolated by the GPU where the radiance and false-colour temperature calculations are then performed at the pixel level in the fragment shader. This allows interpolation of temperature values across the modelled spacecraft, as temperature gradients are an important factor in defining thermal behaviour.

On top of this system, a thermal inertia system was added that modified any temperature change that occurs at any vertex. This system works by loading user-defined thermal materials, including a thermal profile described using mathematical functions (the pair of functions used within the prototype are discussed in Section 3.2). Calculations are then performed during the render loop using the thermal properties, old temperature and newly calculated temperature to add a delay to the thermal transition (heating or cooling) process occurring. Different functions can be used for different materials, and even for the heating and cooling of the same material: this allows the coverage of a wide range of thermal responses. Additionally, different meshes within a model can be assigned different materials, a requirement for simulating complex models like spacecraft.

The calculations performed during the render loop are specified by the user as the thermal profile of a material by defining the coefficients of the chosen function type. To simplify development, the linear function and quadratic polynomial function were chosen to give clear examples that match the requirements from Section 2.3. In future, an extended system could accept any function type: linear; polynomials of any size; exponential; logarithmic; etc., or data sets, of temperature values and time taken, describing measured thermal responses from materials which would allow the extrapolation of the curve without the need for mathematical description.

#### 3.2 Thermal Inertia Effect Equations

In the prototype, a sample set of user-defined functions were used to simulate the thermal inertia effect within a material when a temperature transition occurs. These functions were designed to be controlled using three variables, i.e. an initial temperature, a final temperature and the time-steps



taken to complete the transition (i.e. heat or cool). This allows the creation of a thermal transition within a specified time period, in order to more accurately model the desired thermal response of the chosen material.

Equations 1 and 2 are the linear functions used in the prototype to describe the thermal inertia effect when heating and cooling respectively. The resulting temperature ' $T$ ' at time step ' $t$ ' is described in terms of initial and final temperatures, ' $T_{max}$ ' and ' $T_{min}$ ', and the time-steps taken to complete the transition, ' $t_{max}$ '.

$$T = \left( \frac{T_{max} - T_{min}}{t_{max}} \right) \times t + T_{min} \quad (1)$$

$$T = \left( \frac{T_{min} - T_{max}}{t_{max}} \right) \times t + T_{max} \quad (2)$$

Equations 3 and 4 are the quadratic functions used in the prototype to describe the thermal inertia effect when heating and cooling respectively. The resulting temperature ' $T$ ' at time step ' $t$ ' is described in terms of initial and final temperatures, ' $T_{max}$ ' and ' $T_{min}$ ', and the time-steps taken to complete the transition, ' $t_{max}$ '.

$$T = \left( \frac{T_{min} - T_{max}}{t_{max}^2} \right) \times t^2 + \left( \frac{-2 \times (T_{min} - T_{max})}{t_{max}} \right) \times t + T_{min} \quad (3)$$

$$T = \left( \frac{T_{max} - T_{min}}{t_{max}^2} \right) \times t^2 + \left( \frac{-2 \times (T_{max} - T_{min})}{t_{max}} \right) \times t + T_{max} \quad (4)$$

## 4 RESULTS & EVALUATION

### 4.1 Prototype Evaluation

In Figure 5, the prototype demonstrates quadratic transitions across varying time periods and temperature ranges:

1. Heating from  $2.7K$  to  $267K$  across the entire orbit (361 time steps) - i.e. a slow rise across a long time period
2. Heating from  $2.7K$  to  $267K$  faster than the orbit (100 time steps) - i.e. a rise across a small time period
3. Heating from  $2.7K$  to  $267K$  slower than the orbit (1000 time steps) - i.e. a slow rise across a long time period, longer than the simulation
4. Cooling from  $500K$  to  $2.7K$  across the entire orbit (361 time steps) - i.e. a slow decline across a long time period
5. Cooling from  $500K$  to  $2.7K$  faster than the orbit (100 time steps) - i.e. a decline across a small time period
6. Cooling from  $500K$  to  $2.7K$  slower than the orbit (1000 time steps) - i.e. a slow decline across a long time period, longer than the simulation

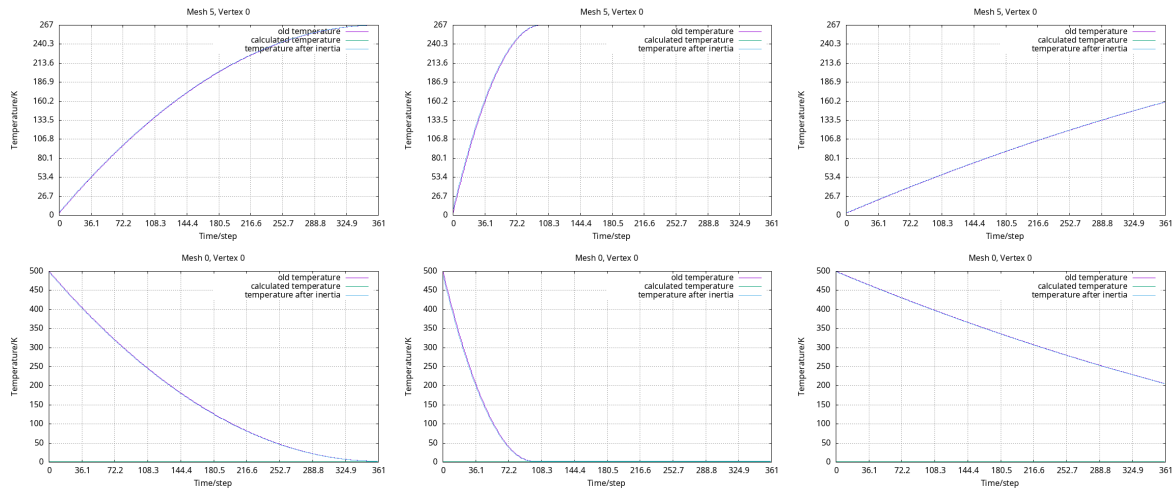


Figure 5: Prototype temperatures graphs using quadratic thermal inertia equation, demonstrating variable conditions

The graphs of Figure 5 demonstrate the ability of the prototype to simulate a variety of thermal transitions according to controllable input parameters.

In Figure 6 the prototype demonstrates smooth transitions in smaller time periods - particularly across extremely high and low temperature ranges:

1. Heating from 2.7K to 1000K faster than the orbit (100 time steps) - i.e. a steep rise across a small time period
2. Cooling from 1000 to 2.7K faster than the orbit (100 time steps) - i.e. a steep decline across a small time period
3. Heating from 2.7K to 5K faster than the orbit (100 time steps) - i.e. a small variation across a small time period
4. Cooling from 5K to 2.7K faster than the orbit (100 time steps) - i.e. a small variation across a small time period

Images 1 and 2 of Figure 6 are examples of an extremely responsive material, similar to the MLI material within ESATAN, while images 3 and 4 are examples of small, slow variations - similar to the Aluminium material within ESATAN.

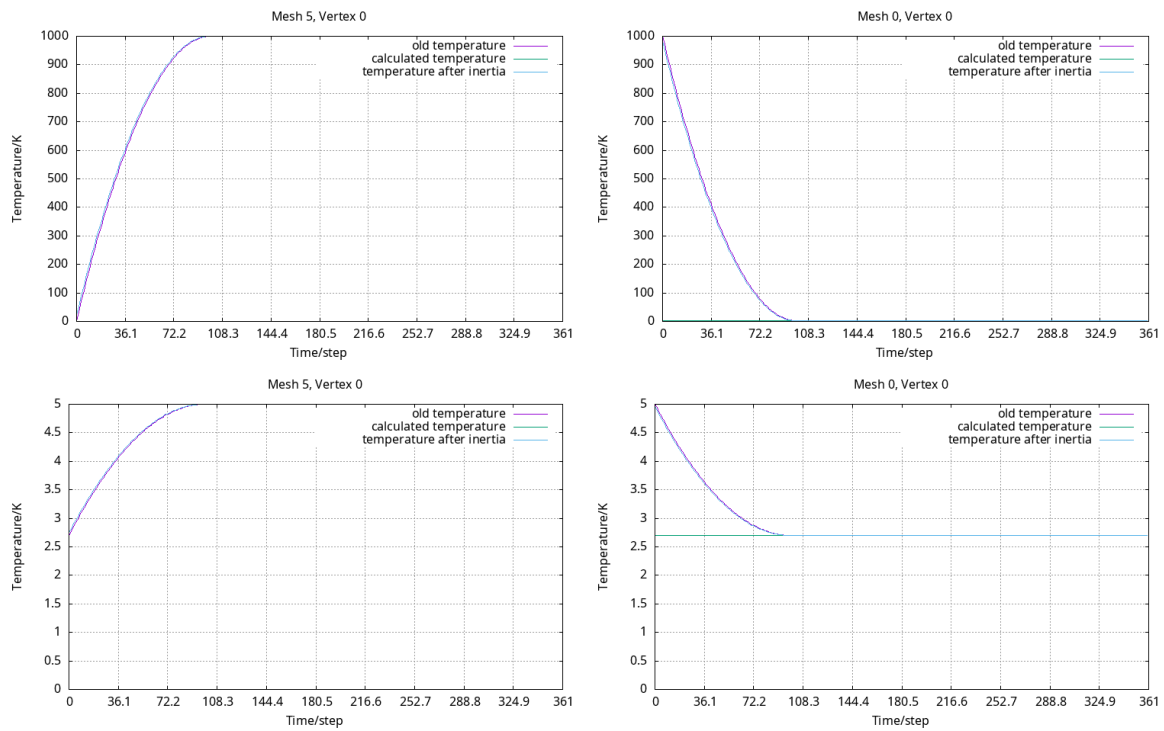


Figure 6: Prototype temperatures graphs using quadratic thermal inertia equation, demonstrating smooth transitions

## 4.2 Complex Models

A good example of the potential of the prototype system is show geometrically complex models, ideally with multiple defined thermal materials. To do so, we can use an ISS model created by NASA [7], seen in VIS and false-colour temperature in Figure 7. Within the TIR image, the darker sections represent lower temperatures and lighter sections represent higher temperatures.

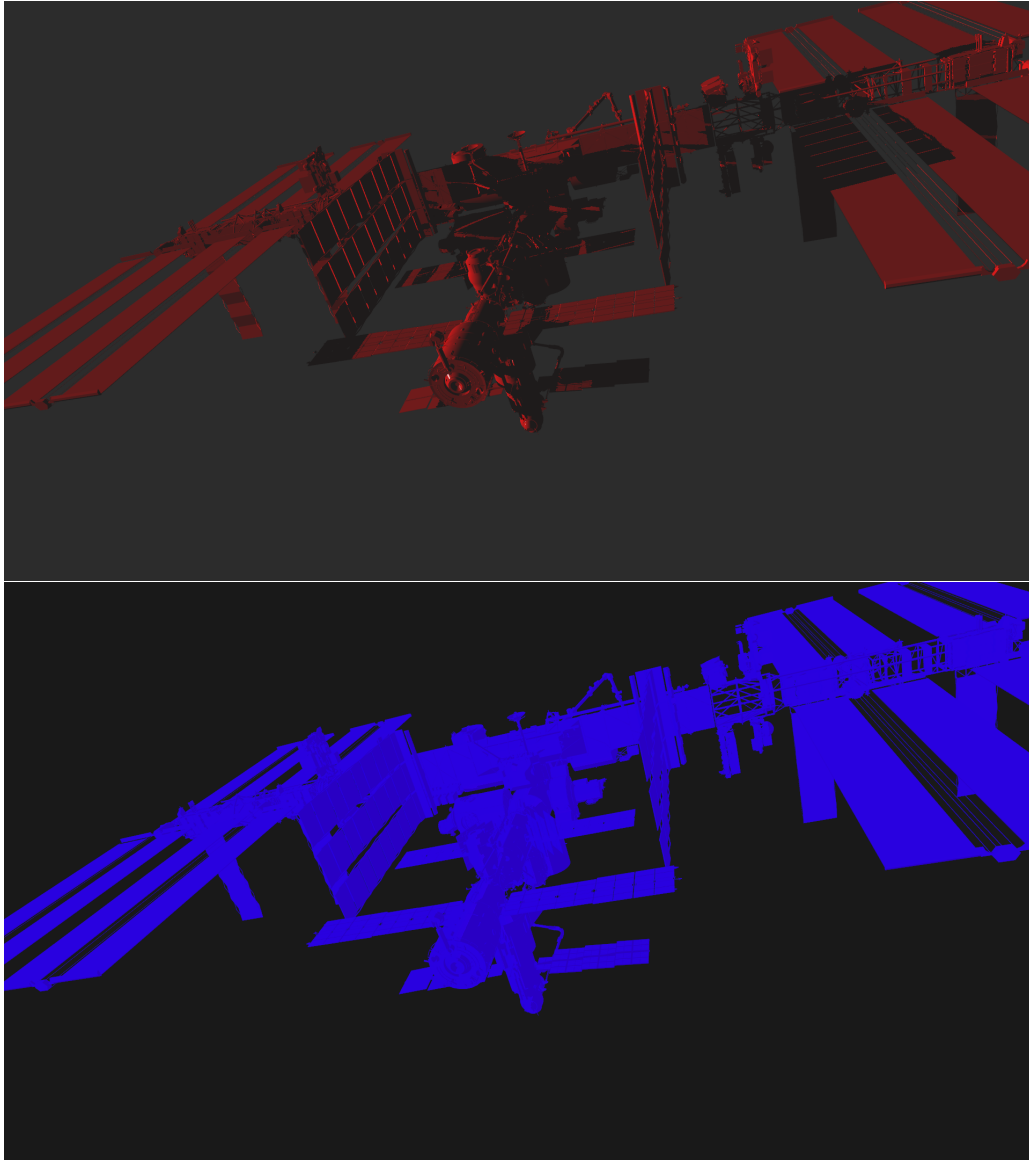


Figure 7: VIS models 1: ISS Model (VIS mode) 2: ISS Model (TIR false-colour temperature mode)

## 5 CONCLUSION

In conclusion, we can use the simulation of thermal inertia to achieve more realistic synthetic images of spacecraft in real time. The examples of the prototype developed shown in Section 4.1 demonstrate that this is possible for a multitude of conditions. In future, these thermal profiles could be combined to create complex thermal profiles, for example complex moments like the entry/exit of eclipse, activation/deactivation of a thermal control system, or spacecraft movements like rotation, extension of solar panels, etc. Simulations of thermal systems would be aided by the creation of publicly available material data sets, in which general properties of the material like density, thermal conductivity, emissivity and absorptivity are described – these are generally lacking in the public domain. The addition of this more accurate thermal system to existing image generation tools could offset this lack of data through the creation of accurate synthetic data, improving existing ‘stateless’ techniques by the addition of consideration of effects that occur over time.

## REFERENCES

- [1] I. Martin, Dunstan, S. M. Parkes, M. Sanchez-Gestido, and G. Ortega, “Simulating planetary approach and landing to test and verify autonomous navigation and guidance systems,” *10th International ESA Conference on Guidance, Navigation & Control Systems (ESA GNC)*, vol. GNC, p. 15, 2017.
- [2] R. Brochard, J. Lebreton, C. Robin, *et al.*, “Scientific image rendering for space scenes with the surrender software,” *arXiv preprint*, 2018. DOI: 10.48550/arXiv.1810.01423.
- [3] J. Rebis and C. Stroom, “Esatan, a review after four years in use (sae technical paper 891558),” *SAE International*, 1989. DOI: 10.4271/891558.
- [4] D. Systems, *Solidworks*, <https://www.solidworks.com/>, (Last Accessed: 25/08/2022).
- [5] I. Martin, M. Dunstan, D. Vural, and M. Sanchez-Gestido, “Simulating thermal infrared images of planets, asteroids and spacecraft,” in *8th International Conference on Astrodynamics Tools and Techniques (ICATT)*, (Jun. 23–25, 2021), vol. ICATT, Virtual, 2021, p. 14.
- [6] C. Savage, “Spacecraft systems engineering,” in John Wiley & Sons Ltd., 2003, ch. 11 - Thermal Control of Spacecraft, pp. 355–391.
- [7] ZeroFrost, *Fixed iss made by nasa*, 2018. [Online]. Available: <https://blenderartists.org/t/fixed-iss-made-by-nasa/1127087>.